Communications Earth & Environment https://doi.org/10.1038/s43247-026-03188-6

Article in Press

Evidence for diverse anaerobic metabolisms in 3.7-billion-year-old marine detrital sediments

Received: 4 June 2025

Accepted: 5 January 2026

Cite this article as: Boyd, A.J., Harding, M.A., Bell, E.A. *et al.* Evidence for diverse anaerobic metabolisms in 3.7-billion-year-old marine detrital sediments. *Commun Earth Environ* (2026). https://doi.org/10.1038/s43247-026-03188-6

Austin Jarl Boyd, Magnus August Ravn Harding, Elizabeth Ann Bell, Minik Thorleif Rosing & Tue Hassenkam

Evidence for diverse anaerobic metabolisms in 3.7-billion-year-old marine detrital sediments

Austin Jarl Boyd*[1], Magnus August Ravn Harding[1], Elizabeth Ann Bell[2], Minik Thorleif Rosing[1], Tue Hassenkam[1]

[1]Globe Institute, University of Copenhagen, Øster Voldgade 5-7, 1350 København, Denmark

[2]Dept. of Earth, Planetary, and Space Sciences, University of California at Los Angeles, 595 Charles E. Young Dr. East/3806 Geology Building, Los Angeles, CA 90095, United States

*Corresponding author: austin.boyd@sund.ku.dk

Abstract

Abundant graphitized organic matter within 3.7-billion-year-old sediments in the Isua Supracrustal Belt comprises the oldest remnants of life. This organic matter could have provided a favorable substrate for anaerobically respiring microbes, though their existence in the early Archean remains uncertain. Here we assess whether anaerobic respiration, linked to reduction of iron and sulfur, operated within these ancient sediments. We analyzed carbon and sulfur isotope data from pelagic and turbiditic sedimentary rocks, sampled from a rock core, and used petrography and iron concentrations to provide geological context. Carbon isotopic compositions indicate respiration of organic compounds, with lighter values associated with iron-rich samples, consistent with respiration coupled to iron reduction. Sulfide grains in pelagic layers have isotopic compositions consistent with reduction of atmospherically produced elemental sulfur, possibly with minor contributions from sulfate reduction during sedimentary hiatuses. These results suggest that early Archean ecosystems were sustained by multiple, interacting microbial metabolisms.

Introduction

The >3.7 Ga Isua Supracrustal Belt (ISB) contains the oldest biogenic carbonaceous matter, preserved within detrital metasedimentary rocks[1–4]. These metasediments accumulated below wave-base, by slow settling of fine pelagic particles, interrupted by turbidity currents carrying particles from nearby edifices[1,5]. A ca. 50m conformable sequence of these metasediments contains several protracted pelagic intervals with abundant graphite that has light carbon isotopic compositions consistent with derivation from photosynthetic organisms[1,4–6]. Continuous high biological productivity in this environment may have been sustained by nutrients in runoff from nearby exposed land[5].

Within modern seafloors, organic matter is remineralized by microorganisms through a variety of metabolic processes. If oxygen is present, it enables aerobic respiration, but in anoxic zones below the seafloor, microbes use other oxidants for respiration. These include nitrous compounds, manganate minerals, ferric iron (Fe^{3+}) and

sulfate[7,8]. These metabolisms are often linked to the oxidation of organic acids or methane, formed by methanogens and fermenters that use organic matter as both reductant and oxidant [8,9].

In modern oceans almost a third of all organic matter that reaches the seafloor is consumed during microbial sulfate reduction[9], but evidence for Archean microbial sulfate reduction occurs only sporadically and only as far back as 3.5 Ga[10,11]. The scarcity of these occurrences is likely a consequence of low sulfate concentrations in the ocean before the rise of atmospheric oxygen[12–14]. In contrast, Fe^{3+} may have been much more abundant within the Archean seafloor. During the Archean, predominant anoxia allowed solute transport of ferrous iron (Fe^{2+}) in the ocean[15]. Phototrophic iron oxidation in the photic zone exported oxidation power to the sediment by precipitation of Fe^{3+}-bearing minerals[16,17]. Such Fe^{3+}-minerals would allow for microbial respiration of organic matter coupled with reduction of Fe^{3+}, also known as dissimilatory iron reduction (DIR). Evidence for this process has been found throughout the Archean[18–23], albeit with the strongest evidence in the late Archean. When and how the sub-seafloor ecosystem developed these diverse metabolic strategies is still an open question[24].

The abundant organic carbon deposited within the precursors of the ISB detrital metasediments would have created an environment suited for microbial anaerobic respiration. These metasediments may therefore provide a window into the complexity of Eoarchean life, allowing us to determine whether complex ecosystems, combining respiration with metabolic strategies that involve the reduction of various ferric and sulfur compounds, had already developed by >3.7 Ga. To determine this, we measured the carbon isotopic composition of graphitic layers and used secondary ion mass spectrometry to determine the in situ sulfur isotopic compositions of individual sulfide grains from a drill core from the ISB. The core covers ca. 50 m of detrital and chemical metasediments, culminating in a depositional contact with the volcanic basement (Fig. S1)[5]. We combine these isotopic measurements with analysis of iron concentration variation within the sedimentary pile and interpret the isotopic and compositional data in relation to their petrographic context. Mineral identification is carried out by a combination of optical microscopy, energy dispersive X-ray spectroscopy and Raman spectroscopy and representative spectra are found in the Supplementary Information (Figs. S4-S7). A description of our sample suite and its geological setting can similarly be found within the Supplementary Information (Supplementary Notes 1-4).

Results

Carbon isotopic evidence for microbial respiration

Total organic carbon (TOC) in our samples varies between 0.11% and 0.96%. Lithologies formed through pelagic deposition span the complete range of TOC values, whereas those formed through turbiditic processes generally have lower concentrations (Fig. 1a). $\delta^{13}C$ varies from −17.7‰ to −36.9‰, with heavier values generally associated with higher TOC (Fig. 1a). The measured $\delta^{13}C$ range extends to values much lower than previously reported in bulk detrital metasedimentary samples from the ISB (−25.6‰ to −12.5‰)[1,2,6,25]. Eleven of our samples have whole-rock $\delta^{13}C$ values that are lighter than −30‰, which is the lightest shift in $\delta^{13}C$ expected for organic matter derived from phototrophic microbes[26], and considerably lighter than the ca. −25‰ average shift from marine carbonate recorded in sedimentary organic material, at any given time from 3.5 Ga to the modern day[27]. If the original $\delta^{13}C$ was between

−25‰ and −30‰, the values that are lower than −30‰ could have formed through respiration of biomass within the sediments. This can lower the $\delta^{13}C$ of the residual carbon by a few permil[28–31]. It is however difficult to explain $\delta^{13}C$ as light as −36‰ through this process and it is therefore likely that carbon with $\delta^{13}C$ equal to or lighter than −36‰ was fixed within the sediment after deposition. Such light carbon is commonly produced where methane has been oxidized through anaerobic respiration or has been incorporated into organic molecules[24,32], and, as such, similarly light $\delta^{13}C$ values of less than −35‰ in younger Archean organic matter have been explained by metabolic processes involving methane[19,32]. Methane could have formed through biologically mediated processes of fermentation and methanogenesis within oxidant-depleted parts of the seafloor. It could then have seeped up into more oxidant-rich sediments where methanotrophs would have produced secondary biomass using those oxidants.

Previous in-situ measurements, from the same rock core, have found graphitic carbon, isolated within post-depositional mineral phases, with $\delta^{13}C$ as light as −33.7‰[4]. These occurred near graphite with $\delta^{13}C$ as heavy as −13.9‰, suggesting that considerable heterogeneous post-depositional carbon isotopic fractionation occurred early in the sediment's history, before the growth of mineral phases formed during later metamorphism. As such, the lightest bulk $\delta^{13}C$ values measured in our samples may represent layers where, prior to metamorphic equilibration, a larger proportion of carbon consisted of the lighter fraction isolated and observed within post-depositional mineral phases. Early and heterogeneous formation of these lightest bulk $\delta^{13}C$ values would be consistent with formation during sub-seafloor metabolic processes. The relationship between $\delta^{13}C$ and TOC (Fig. 1a) suggests that the absolute amount of organic matter affected by these processes was limited, e.g., by the amount of ferric iron, sulfate or other electron acceptors accessible to the microbes.

We would expect the metabolic respiratory processes described above to produce bicarbonate during the oxidation of methane and organic acids, which could lead to precipitation of diagenetic carbonate. Indeed, calcite commonly occurs in a petrographic context that is consistent with post-depositional formation within the seafloor. In pelagic layers it occurs as nodules and in horizons that follow the sedimentary bedding (Fig. 2a), whereas some turbiditic layers contain calcite nodules and truncated veins. Calcite from hand samples of the turbiditic units have $\delta^{13}C$ values from −7.3‰ to −9.8‰ (n = 3)[33] and calcite formed within pelagic sections of the core have $\delta^{13}C$ values of −3.0‰ to −6.3‰[4]. These values are lighter than what would be expected for pure seawater precipitates[20,23,27], which is consistent with some amount of bicarbonate being derived from microbial respiration of methane, and/or organic acids[32,34,35].

Given that the samples have experienced multiple episodes of amphibolite-facies metamorphism (see Supplementary Notes 1-2), it is necessary to assess whether metamorphic or abiotic processes could have influenced or produced the observed carbon isotopic compositions. In other parts of the ISB, graphite formation has been attributed to the disproportionation of siderite into magnetite and graphite, yielding $\delta^{13}C$ values of −10‰ to −12‰[36]. However, this process is not relevant to the samples described here, as high TOC samples would be associated with high concentrations of magnetite and the associated fractionation would not be enough to form even the heaviest $\delta^{13}C$ values measured here (−17.7‰). Another possibility is that carbon isotopic compositions were altered during metamorphism. Previous in-situ $\delta^{13}C$ measurements of graphite grains for this sample suite[4], mentioned above, show that graphite grains trapped within some metamorphic grains actually have lighter and more heterogeneous $\delta^{13}C$ than

graphite in the matrix. This suggests that the graphitic $\delta^{13}C$ was homogenized, generally obscuring the presence of lighter values. There is also the possibility that some or all the organic matter and its isotopic composition could have formed through abiotic reactions. In particular, carbon isotopes can become fractionated through Fischer-Tropsch style processes where CO_2 is reduced to methane and other short organic molecules in the presence of hydrogen[37], a process that has been documented in hydrothermal systems associated with the hydration of ultramafic rocks. However, this mechanism is inconsistent with the high concentrations of nitrogen, bound with both graphite and mica, within the detrital metasediments[3,5,38]. Moreover, if graphite entered the sediments through this process, we would expect to find it associated with veins cutting across the sedimentary layers. Instead we observe that graphite concentrations vary only between the layers (Fig. 2a, c, d)[5].

Ferric iron as electron acceptor during microbial respiration

As discussed above, carbon isotopic compositions for graphite and carbonate are consistent with microbial respiration taking place after sediment deposition, but they do not reveal which oxidants were used in the process. One likely metabolic mechanism is DIR, which utilizes ferric iron[18]. Our XRF data, combined with previously published ICP-MS data[5], show that Fe concentrations are variable, but consistently high in the lower metasediments (see Supplementary data 3), reaching concentrations of 37 wt.%. The same pattern persists after normalization of Fe concentrations to Al or Ti (Fig. S1), consistent with a contribution of iron from precipitation of dissolved iron species[15,23]. High Fe concentrations in Archean sediments do not, by themselves, demonstrate that ferric iron was available, since Fe^{2+} could also have precipitated directly from ferruginous seawater. However, Fe-isotope analyses of other similar Archean ferruginous siliciclastic sediments, combined with experimental constraints, indicate that such Fe enrichments are best explained by oxidative precipitation of Fe^{3+}-minerals[23]. Fe concentrations decline upwards in the core, but there are frequent returns to elevated values throughout the sedimentary layers, including millimeter-thick layers composed of clinozoisite or epidote grains (both Fe^{3+}-bearing; Fig. 2b). These layers are sometimes associated with calcite and sulfides, consistent with respiration being enhanced by the presence of Fe^{3+}.

If Fe^{3+} reduction played a major role in the respiration of organic matter, lighter $\delta^{13}C$ values would be expected in layers with higher iron concentrations, relative to organic matter. On the other hand, layers with high abundances of pelagic organic carbon would, on average, have retained their original isotopic composition. Indeed, Fe/TOC ratios plotted against $\delta^{13}C$ (Fig. 1b) show that samples with lower Fe/TOC tend to have heavier $\delta^{13}C$ values, while those with higher Fe/TOC show lighter values. This negative trend is consistent with microbial respiration fueled by DIR. The existence of DIR during deposition of sedimentary sequences within the ISB has been suggested before, based on the iron and carbon isotopic composition of carbonates within BIFs[20] and on the iron isotopic composition of sulfides[21], but due to metamorphic alteration it is unclear if these isotopic signals could be linked to metabolic activity within sediments[22]. In contrast, our carbon isotopic data were derived from samples with bona fide sedimentary protoliths

with carbonaceous matter deposited within the original sedimentary environment[5]. As such, our data are fully consistent with DIR taking place within the seafloor at 3.7 Ga.

Petrographic evidence for microbial reduction of sulfur compounds

Although the trend observed in Fig. 1b suggests that the amount of Fe available to perform DIR determined how much oxidation of methane and/or organic acids could take place within the sediment, there is considerable dispersion along the trend. In particular, some samples have relatively light $\delta^{13}C$ values, but comparatively low or moderate Fe/TOC ratios, which may be related to metabolic processing independent of ferric iron.

Abundant occurrence of sulfides in graphite-rich layers hints that respiration may have been coupled to the reduction of sulfur species, forming H_2S. Most sulfides occur along discrete sedimentary layers (Figs. 2a, c-d) and consist mainly of pyrrhotite, with lesser pyrite and rare pentlandite or chalcopyrite (see SI for representative EDS spectra). Pyrrhotite is interpreted as a metamorphic phase, formed by recrystallization of primary diagenetic sulfides in seafloor sediments. This interpretation is consistent with the low abundance of Cu- and Ni-bearing sulfides, as these phases are scarce in low-temperature diagenetic assemblages[39], but typically mobilized from rocks during high-temperature (>300 °C) hydrothermal fluid flow[40].

Most sulfides have no internal texture and irregular grain boundaries defined by the surfaces of neighboring grains, but some pyrite grains occur as rounded concretions consisting of concentric zones of pyrite delineated by micron-sized inclusion trails (Fig. 2e). These grains mostly occur in iron-rich layers and are often disseminated throughout millimeter-scale beds, rather than confined to layer boundaries. Such concentric textures resemble pyrite formed during syn-sedimentary or early diagenetic conditions in younger sedimentary rocks[41]. Consistent with this interpretation, diffusion-reaction modelling indicates that these features can develop along reaction fronts between Fe-rich and H_2S-rich fluids within permeable sediments[42], a process that also produces sulfide bands along sedimentary boundaries, similar to the bands of sulfides observed along sedimentary layers in our sample suite (Fig. 2a, c, d)[43]. We therefore suggest that horizontal sulfide layers formed where upward-diffusing H_2S encountered Fe-rich seawater at the sediment-water interface. In contrast, the disseminated concentric pyrite concretions may reflect environments where Fe^{2+} was produced within the sediment through DIR in layers richer in Fe^{3+}-bearing minerals. Taken together, the mineralogy, textures, and structural distribution of sulfides point to an early diagenetic origin that was subsequently modified by metamorphic recrystallization.

Sulfides are typically abundant in the graphitic pelagic sections whereas turbiditic sections contain few, if any, sulfides. Since turbiditic sections are primarily composed of crustal particles, the uneven distribution of sulfides between these two sedimentary facies indicates that most sulfur did not originate directly from crustal material. Further, the abundant occurrence of sulfides within highly graphitic samples suggests that sulfide formation was linked to the carbonaceous matter in the sediments, which could have acted as an electron donor during the reduction of

sulfur compounds in the sediments. This is also consistent with the frequent co-occurrence of sulfides with calcite, which would precipitate during the oxidation of carbonaceous matter (Figs. 2a, 3).

The occurrence of sulfides along discrete horizons in pelagic sections suggests that detrital accumulation rates influenced where and how much sulfide formed. The sulfides are commonly observed in quartz-rich layers, interbedded with muscovite- and chlorite-rich layers (Figs. 2a, c), which likely represent depositional periods characterized by slow accumulation of chert and faster accumulation of detrital clays, respectively. Similarly, the occurrence of sulfide grains and clusters along the boundary of two layers, sometimes contiguously for several centimeters (Fig. 2d), indicate that sulfide formed during a hiatus in sedimentary deposition. These patterns are consistent with a scenario where sulfides formed during intervals of slow sedimentation, where pore fluids enriched in dissolved sulfide, formed through sulfur-based respiration, diffused upwards and reacted with seawater Fe^{2+} as described above. In the cases where sulfides occur within layers, especially where concentric pyrite nodules are observed, these may have formed deeper in the sediments within layers with high concentrations of Fe^{3+} allowed for the continuous production of Fe^{2+} through DIR.

Sulfur isotopic tracing of sulfur species

To further investigate whether and how microbial reduction of sulfur species was occurring, we used secondary ion mass spectrometry to analyze the sulfur isotopic composition of individual sulfide grains (pyrrhotite, pyrite, pentlandite, and chalcopyrite; see Fig. S6 for representative EDS spectra) within selected sedimentary layers. Mass-dependent sulfur isotope fractionation is expressed by the $\delta^{34}S$ value (defined in Methods section). In Archean samples, the speciation of seawater-derived sulfur can be traced using the deviation from mass-dependent fractionation of sulfur isotopes, which is expressed using the $\Delta^{33}S$ value. Archean variations in $\Delta^{33}S$ are derived from photochemical disproportionation of SO_2 gas in the atmosphere, which produces particulate elemental sulfur (S^0) with positive $\Delta^{33}S$ and soluble sulfate (SO_4^{2-}) with negative $\Delta^{33}S$ (Fig. 3)[10,44,45]. The Archean Reference Array is an empirical $\delta^{34}S$–$\Delta^{33}S$ trend in measurements for Archean sulfides and is interpreted to reflect variable dilution of photochemically produced S^0, with SO_4^{2-}, or with mantle-derived sulfur[46]. Our samples all show positive $\Delta^{33}S$ values (+0.4‰ to +3.2‰; Fig. 4) and plot close to the Archean Reference Array, with most $\delta^{34}S$ values plotting 0–4‰ lower than the array, although a few measurements with low $\Delta^{33}S$ are up to 1‰ higher. The uniformly positive $\Delta^{33}S$ values indicate a consistent contribution to the sulfur budget from S^0-particulates that formed in the atmosphere. Microbes in modern settings use elemental sulfur as an oxidant during respiration[47,48] and both genomic and isotopic data have shown that this metabolism developed early in the history of life[49,50]. Given the petrographic evidence that sulfide formation was syn-sedimentary, it is possible that this metabolic strategy was being employed by microbes within these sediments. Microbial reduction of elemental sulfur typically only produces minor $\delta^{34}S$ fractionation (<5‰)[48], consistent with our data. However, elemental sulfur can also undergo microbial disproportionation, in which sulfur is partitioned into both reduced (H_2S) and oxidized (SO_4^{2-}) species. In this case, the produced sulfate could subsequently be reduced to H_2S, yielding the same overall chemical products as direct S^0 reduction. This process generally yields greater sulfur isotope fractionations than those observed here[51], but any original isotopic spread could have been narrowed by isotopic

equilibration during diagenetic or metamorphic overprint. Thus, while the sulfur isotope systematics are consistent with microbial S^0 reduction, microbial S^0 disproportionation cannot be excluded.

The variation in $\Delta^{33}S$ values between +0.4‰ and +3.2‰ may suggest that, in addition to the microbial reduction of elemental sulfur with high $\Delta^{33}S$, metabolisms using other sulfur sources with low $\Delta^{33}S$ may have occurred. The variation primarily occurs between layers, suggesting real shifts in the relative contribution of sulfur sources through time, possibly due to changes in depositional conditions. Most layers have $\Delta^{33}S$ values between +1‰ and +2‰, whereas the deepest measured layer shows distinctly higher values and a few isolated layers exhibit lower ones. Several of the layers with intermediate compositions are separated by only a few centimeters, share similar lithological characteristics and nearly identical $\Delta^{33}S$ values, indicating that sulfur source contributions varied gradually or with changes in depositional character.

A potential cause for the dilution of the high-$\Delta^{33}S$ elemental sulfur signal is input of sulfur from crustally derived erosional products. However, as discussed above, the uneven distribution of sulfides between pelagic and turbiditic facies indicates that such crustal input contributed little to the overall sulfur budget of these samples. Another possibility is that sulfur entered the sediments with volcanic or hydrothermal material, derived from subaqueous volcanic vents. However, we observe the most positive $\Delta^{33}S$ value in the deepest sample, which was deposited closest in time to the formation of the volcanic basement[5]. In fact, the high iron concentrations measured within the deepest sediments (Fig. S1) could be related to greater Fe-precipitation rates caused by hydrothermal addition of dissolved Fe^{2+} to the ocean while subaqueous volcanism was still active[5,52]. Similarly high $\Delta^{33}S$ values have been measured within iron-rich sediments elsewhere in the ISB (Fig. 4)[53,54], suggesting that the conditions that lead to high iron sedimentation also inhibit the dilution of sulfide derived from elemental sulfur by other sulfur sources. There is therefore no indication that volcanic or hydrothermal sulfur caused the dilution of the positive $\Delta^{33}S$ elemental sulfur signal in our samples.

Given the lack of evidence for other sources of sulfur, microbial reduction of seawater sulfate is the most likely cause of $\Delta^{33}S$ variation toward lower values. However, evidence for microbial sulfate reduction is typically linked to negative $\Delta^{33}S$ values and/or large variations in $\delta^{34}S$ (>10‰)[11]. The range in $\delta^{34}S$ for our whole sample suite is only ca. 5‰ and within a single layer, the greatest range is 3.8‰ (Fig. 4). However, sulfate reduction would produce only small variations in $\delta^{34}S$ if the sulfate pool was small enough for reduction to be near-complete. Habicht et al.,[13] observed that sulfides formed during sulfate reduction from water with <200 µM sulfate only would display minor fractionation of the $\delta^{34}S$ value, whereas Crowe et al.[14] demonstrated that sulfate concentrations of <5 µM sulfate would be required to explain the low degree of mass dependent sulfur isotope fractionation observed in most Archean samples. Both studies observed that microbial sulfate reduction could take place in sediments at micromolar levels of sulfate concentration, resulting in $\delta^{34}S$ compositions spanning less than 10‰. It is therefore possible that porewater sulfate was reduced quantitatively and continuously replenished during periods of slow detrital deposition. Formation of low $\Delta^{33}S$ sulfide from the reduction of sulfate in slowly accumulating sediments is supported by the petrographic context of samples that display these low $\Delta^{33}S$ values. These samples consist of quartz-rich beds, consistent with the

accumulation of chert during periods of slow detrital sedimentation, and are comparatively sulfide-rich (e.g. Fig. 2e), possibly owing to the longer period of time for sulfate to enter the porewater.

Recently measured negative $\Delta^{33}S$ values from the northeastern ISB demonstrate that sulfate-derived sulfides could accumulate within the seafloor of the basin in which the ISB formed[55] (Fig. 4). The $\delta^{34}S$ values of these sulfides (+1‰ to +2‰) also correspond closely to those expected for Archean sulfate-derived H_2S, consistent with our interpretation that the isotopic array of our samples reflects mixing between H_2S produced by elemental sulfur reduction and by microbial sulfate reduction. The $\delta^{34}S$ composition of the ambient seawater sulfate reservoir at 3.7 Ga is not well constrained, but it was likely slightly positive, reflecting a small, dynamic sulfate pool that was continually buffered by isotopically lighter sulfate supplied from the atmosphere. This interpretation is supported by $\delta^{34}S$ values of +2‰ to +7‰ reported for Paleoarchean sulfate minerals[56,57]. As such, the relatively narrow and near zero $\delta^{34}S$ values observed in our samples and in the northeastern ISB sulfides are consistent with variable amounts of sulfur being derived from near-quantitative reduction of sulfate from a small sulfate pool.

Discussion

Previous petrographic description of our sampled rock core (Boyd et al., 2024) and high-resolution iron concentration measurements (Fig. S1; Supplementary data 3) have shown that the Eoarchean Isua basin experienced a gradual change in depositional characteristics. Initial deposition consisted of ferric or mixed valence iron precipitates, coincident with detrital aluminosilicate particles (Fig. S3b and Fig. S3c), which graded into deposition that was mostly dominated by detritals (Fig. S3a, Fig. S3d and Fig. S3e), but with occasional pulses of ferric chemical precipitates. Pelagic sedimentary layers with organic matter also became more prevalent after the rate of iron deposition declined, forming a seafloor where ferric iron–rich and organic carbon–rich layers often occurred in close proximity. Our measured $\delta^{13}C$ values show that the accumulated organic matter allowed for the microbial oxidation of primary organic material, methane, and/or organic acids, and the negative trend with iron is consistent with Fe^{3+} acting as an oxidant in this process (Figs. 1, 3). The frequent occurrence of layers with abundant sulfides, exclusively found within carbonaceous sedimentary sections formed by slow pelagic accumulation, suggests that microbial reduction of sulfur compounds also contributed towards the respiration of carbonaceous matter. The sulfur isotopic composition of sulfides shows that a large proportion of the sulfur was derived from elemental sulfur, but that it was variably mixed with sulfur derived from other sources. It is likely that the remaining sulfur was derived from the near-quantitative microbial reduction of sulfate.

Other studies have similarly ascribed the dominantly positive, but variable $\Delta^{33}S$ observed throughout time and within specific localities to mixing of sulfur derived from elemental sulfur and sulfate[45,58,59]. Farquhar et al.[59] proposed that positive $\Delta^{33}S$ values prevail in Archean shales because they formed in marginal basins where nearby volcanic activity increased atmospheric SO_2 concentrations, promoting the formation of short-lived particulate elemental sulfur that preferentially settled into deeper parts of the basin. In contrast, the co-produced sulfate was more broadly distributed, and its local concentration may have been diminished by hydrothermal scavenging within the seafloor. The remaining low levels of sulfate would be available for microbial sulfate reduction within organic-rich sediments, producing lower

cumulative $\Delta^{33}S$ values. As such, this model could explain the interlayer $\Delta^{33}S$ variability we observe. The highest values occur in the sample closest to the volcanic basement and within ISB iron formations[53,54], which likely formed during enhanced Fe^{2+} exhalation from hydrothermal vents[52]. Such hydrothermal activity would have scavenged sulfate from seawater through the precipitation of barite or anhydrite, locally depleting the sulfate reservoir and enhancing the relative contribution of elemental sulfur–derived sulfide to the sedimentary sulfur pool. Conversely, the lowest $\Delta^{33}S$ values are observed in layers showing petrographic evidence for depositional hiatuses, where extended porewater residence times may have allowed greater accumulation of sulfate-derived sulfur.

Taken together, the variations in sulfur and carbon isotopes and mineral associations indicate a dynamic redox landscape in the ISB basin, where fluctuations in the availability of Fe^{3+}, sulfate, and elemental sulfur created diverse microbial niches. The isotopic and petrographic evidence suggests that organic matter accumulated on the seafloor and sustained microbial communities that coupled fermentation and oxidation of organic matter with the reduction of ferric iron, elemental sulfur, and sulfate (Fig. 3). These findings imply that by this time, ecosystems composed of multiple interacting metabolic pathways had already evolved.

Methods

Sulfur isotopic measurements

Rock fragments containing sulfides were embedded in six 2.5cm wide epoxy discs and polished in stages using progressively finer diamond grit, finishing with a 0.1µm alumina agent and then a 0.04µm colloidal silica agent. Sulfide mineralogy and placement were determined using a petrographic reflective light optical microscope, and sulfide mineralogy was validated by semi-quantitative elemental compositions measured using energy dispersive X-ray spectroscopy attached to a Tescan Vega-3 XMU variable-pressure scanning electron microscope (see Fig. S6 for representative spectra).

Epoxy discs were gold coated and then degassed within a vacuum chamber before being placed within the holding chamber of a CAMECA ims-1290 secondary ion mass spectrometer at the University of California, Los Angeles. A 1nA Cs+ beam operating at 10kV, was centered on a 10µm x 10µm region of interest, removing the gold coating and sputtering the area for 120 seconds before starting analysis. Secondary ions were accelerated by a −10kV electric field and isotopes of sulfur (^{32}S, ^{33}S and ^{34}S) were detected in multicollection mode via three Faraday cups in 20 acquisition cycles within 120 seconds. The mass resolving power of ~4000 was sufficient to separate interferences, including ^{32}SH. An electron flood gun was used for charge compensation during pre-sputtering and analysis. Analysis took place over 5 days.

Sample measurements were bracketed by measurement of matrix-matched standards that were mounted within another set of epoxy discs and swapped in from the holding chamber. Standards consisted of Balmat for pyrite[60], 7151 for chalcopyrite[61], Anderson for pyrrhotite[61] and BM1975 for pentlandite[62]. Instrumental mass fractionation of the $^{33}S/^{32}S$ and the $^{34}S/^{32}S$ ratios was corrected for each analytical day using the bracketing standards measured that day. The reported 1σ external errors (see Supplementary data 2) include internal errors for each data point, combined in quadrature with the standard deviation (1 SD) of the respective standard measured that day. Data are

reported relative to the Canyon Diablo Troilite (V-CDT) reference value[63], calculated by the following formula: $\delta^{x}S = (((^{x}S/^{32}S)sample/(^{x}S/^{32}S)V\text{-}CDT) -1)\times1000$, where x = 34 or 33, depending on the isotopic ratio in question. The degree of mass-independent fractionation is reported as $\Delta^{33}S$, which is calculated as the deviation from mass dependent covariation of $\delta^{33}S$ and $\delta^{34}S$, i.e.: $\delta^{33}S-\theta\times\delta^{34}S$, where θ represents the slope of $\delta^{33}S$ versus $\delta^{34}S$ during mass dependent fractionation. To reduce uncertainty, θ was determined by linear regression of all standard measurements acquired that day, rather than assuming a fixed value. Instrumental mass fractionation and error bars for reported $\Delta^{33}S$ values were corrected using all standards measured across the analytical day.

Carbon isotopic and elemental concentration measurements

Carbon isotope and total organic carbon measurements were carried out at the University of Copenhagen on 54 rock powder aliquots sampled from various places within the upper two zones of the core. 48 of the powder samples had previously been analyzed for major and trace elemental concentrations[5]. 30 mg of rock powder were weighed out for each sample and carbonate was removed from each sample through acid fumigation using 12M HCl. Samples were transferred to tin capsules, combusted at 1700 °C, and the resultant CO_2 gas was transferred to a Thermo Delta V Advantage (Thermo Scientific) isotopic ratio mass spectrometer and a Flash 2000 (Thermo Scientific) Elemental Analyzer for measurement of $\delta^{13}C$ and TOC respectively. $\delta^{13}C$ analyses were calibrated against ^{13}C-sucrose ($\delta^{13}C$ = −10.4‰; IAEA, Vienna, Austria) and TOC values were calibrated against internal standards consisting of 9.6 mg to 32.0 mg loamy soil. Loamy soil standards were also analyzed in between sample measurements to monitor $\delta^{13}C$ drift.

Compositional X-ray fluorescence measurements

Fe-, Al- and Ti concentrations were measured through portable X-ray fluorescence spectroscopy using an Olympus Vanta M Series XRF Analyzer, with which measurements were taken directly on the rock core. Measurements were taken along the core between 35.82m and 79.83m with variable spacing. Data were collected in the instrument's Geochem mode using a 40kV beam for 60 seconds, a 10kV beam for 120 seconds and a 50kV beam for 30 seconds. Final concentrations were derived from calculations carried out by the Vanta equipment software, which was calibrated using Olympus in-house standards. Data was validated through measurements of NIST certified standard 2711a and by measurement of four powder samples that were derived from the analyzed core and which had previously been analyzed by ICP-MS (reported by Boyd et al.[5]). Fe, Al, and Ti values for powder samples were, on average, within 10% of the values measured by ICP-MS, but the average Al-value of one sample was 21% lower than the ICP-MS value and the average Fe-value of another sample was 14% higher than that measured by ICP-MS. Data and standard measurements are reported within the Supplementary data 3.

Data availability

Sulfur and carbon isotope data, as well as iron, titanium, and aluminum concentrations measured directly on the rock core, are provided in the supplementary data and are also available from the following repository: https://doi.org/10.17894/ucph.62287630-6632-4b1f-9641-ad529d5e8bca

Acknowledgments

We are grateful for assistance provided by Nozomi Matsuda during the acquisition of sulfur isotopic data. This project was made possible through financial support provided by the Novo Nordisk Foundation through NERD grant NNF21OC0068372. Research and export permits for rock core materials were granted by the Greenlandic self-government.

Author Contributions

A.J.B. led the writing of the paper, while T.H. provided regular feedback. A.J.B., T.H., M.A.R.H., and M.T.R contributed to data interpretation. M.T.R. collected the sample material. M.A.R.H., E.A.B., and A.J.B. conducted sample preparation, characterization, and compositional analysis. E.A.B. and A.J.B. carried out data reduction. E.A.B., M.T.R., and T.H. provided analytical equipment and materials. All authors contributed to the editing and review of the paper.

Competing interests

The authors declare no competing interests.

References

1. Rosing, M. T. 13C-Depleted Carbon Microparticles in >3700-Ma Sea-Floor Sedimentary Rocks from West Greenland. *Science* **283**, 674–676 (1999).
2. Ohtomo, Y., Kakegawa, T., Ishida, A., Nagase, T. & Rosing, M. T. Evidence for biogenic graphite in early Archaean Isua metasedimentary rocks. *Nature Geosci* **7**, 25–28 (2014).
3. Hassenkam, T., Andersson, M. P., Dalby, K. N., Mackenzie, D. M. A. & Rosing, M. T. Elements of Eoarchean life trapped in mineral inclusions. *Nature* **548**, 78–81 (2017).
4. Harding, M. A. R. *et al.* Preserved carbon isotope compositions in 3.7 billion year old detrital organic matter from the Isua Supracrustal Belt. *Commun Earth Environ* **6**, 244 (2025).

5. Boyd, A. J., Rosing, M. T., Harding, M. A. R., Canfield, D. E. & Hassenkam, T. 3.7 billion year old detrital sediments in Greenland are consistent with active plate tectonics in the Eoarchean. *Commun Earth Environ* **5**, 201 (2024).
6. Rosing, M. T. & Frei, R. U-rich Archaean sea-floor sediments from Greenland – indications of >3700 Ma oxygenic photosynthesis. *Earth and Planetary Science Letters* **217**, 237–244 (2004).
7. Froelich, P. N. *et al.* Early oxidation of organic matter in pelagic sediments of the eastern equatorial Atlantic: suboxic diagenesis. *Geochimica et Cosmochimica Acta* **43**, 1075–1090 (1979).
8. Orsi, W. D. Ecology and evolution of seafloor and subseafloor microbial communities. *Nat Rev Microbiol* **16**, 671–683 (2018).
9. Bowles, M. W., Mogollón, J. M., Kasten, S., Zabel, M. & Hinrichs, K.-U. Global rates of marine sulfate reduction and implications for sub–sea-floor metabolic activities. *Science* **344**, 889–891 (2014).
10. Ueno, Y., Ono, S., Rumble, D. & Maruyama, S. Quadruple sulfur isotope analysis of ca. 3.5 Ga Dresser Formation: New evidence for microbial sulfate reduction in the early Archean. *Geochimica et Cosmochimica Acta* **72**, 5675–5691 (2008).
11. Shen, Y. & Buick, R. The antiquity of microbial sulfate reduction. *Earth-Science Reviews* **64**, 243–272 (2004).
12. Canfield, D. E., Habicht, K. S. & Thamdrup, B. The Archean Sulfur Cycle and the Early History of Atmospheric Oxygen. *Science* **288**, 658–661 (2000).
13. Habicht, K. S., Gade, M., Thamdrup, B., Berg, P. & Canfield, D. E. Calibration of Sulfate Levels in the Archean Ocean. *Science* **298**, 2372–2374 (2002).
14. Crowe, S. A. *et al.* Sulfate was a trace constituent of Archean seawater. *Science* **346**, 735–739 (2014).

15. Poulton, S. W. & Canfield, D. E. Ferruginous Conditions: A Dominant Feature of the Ocean through Earth's History. *Elements* **7**, 107–112 (2011).

16. Czaja, A. D. *et al.* Biological Fe oxidation controlled deposition of banded iron formation in the ca. 3770Ma Isua Supracrustal Belt (West Greenland). *Earth and Planetary Science Letters* **363**, 192–203 (2013).

17. Kappler, A., Pasquero, C., Konhauser, K. O. & Newman, D. K. Deposition of banded iron formations by anoxygenic phototrophic Fe(II)-oxidizing bacteria. *Geol* **33**, 865 (2005).

18. Johnson, C. M., Beard, B. L., Klein, C., Beukes, N. J. & Roden, E. E. Iron isotopes constrain biologic and abiologic processes in banded iron formation genesis. *Geochimica et Cosmochimica Acta* **72**, 151–169 (2008).

19. Czaja, A. D. *et al.* Iron and carbon isotope evidence for ecosystem and environmental diversity in the ~2.7 to 2.5Ga Hamersley Province, Western Australia. *Earth and Planetary Science Letters* **292**, 170–180 (2010).

20. Craddock, P. R. & Dauphas, N. Iron and carbon isotope evidence for microbial iron respiration throughout the Archean. *Earth and Planetary Science Letters* **303**, 121–132 (2011).

21. Yoshiya, K., Sawaki, Y., Hirata, T., Maruyama, S. & Komiya, T. In-situ iron isotope analysis of pyrites in ~ 3.7 Ga sedimentary protoliths from the Isua supracrustal belt, southern West Greenland. *Chemical Geology* **401**, 126–139 (2015).

22. Marin-Carbonne, J. *et al.* In Situ Fe and S isotope analyses in pyrite from the 3.2 Ga Mendon Formation (Barberton Greenstone Belt, South Africa): Evidence for early microbial iron reduction. *Geobiology* **18**, 306–325 (2020).

23. Suzumeji, R. *et al.* Primary Fe isotope signatures record oxidative precipitation in 3.2 Ga ferruginous siliciclastic sedimentary rocks deposited in a shallow ocean environment. *Precambrian Research* **413**, 107574 (2024).

24. Lepot, K. Signatures of early microbial life from the Archean (4 to 2.5 Ga) eon. *Earth-Science Reviews* **209**, 103296 (2020).

25. Grassineau, N. V., Abell, P., Appel, P. W. U., Lowry, D. & Nisbet, E. G. Early life signatures in sulfur and carbon isotopes from Isua, Barberton, Wabigoon (Steep Rock), and Belingwe Greenstone Belts (3.8 to 2.7 Ga). in *Evolution of Early Earth's Atmosphere, Hydrosphere, and Biosphere - Constraints from Ore Deposits* (Geological Society of America, 2006). doi:10.1130/2006.1198(02).

26. Thomazo, C. *et al.* Biological activity and the Earth's surface evolution: Insights from carbon, sulfur, nitrogen and iron stable isotopes in the rock record. *Comptes Rendus Palevol* **8**, 665–678 (2009).

27. Garcia, A. K., Cavanaugh, C. M. & Kacar, B. The curious consistency of carbon biosignatures over billions of years of Earth-life coevolution. *The ISME Journal* **15**, 2183–2194 (2021).

28. Londry, K. L., Dawson, K. G., Grover, H. D., Summons, R. E. & Bradley, A. S. Stable carbon isotope fractionation between substrates and products of Methanosarcina barkeri. *Organic Geochemistry* **39**, 608–621 (2008).

29. McArthur, J. M., Tyson, R. V., Thomson, J. & Mattey, D. Early diagenesis of marine organic matter: Alteration of the carbon isotopic composition. *Marine Geology* **105**, 51–61 (1992).

30. Freudenthal, T., Wagner, T., Wenzhöfer, F., Zabel, M. & Wefer, G. Early diagenesis of organic matter from sediments of the eastern subtropical Atlantic: evidence from stable nitrogen and carbon isotopes. *Geochimica et Cosmochimica Acta* **65**, 1795–1808 (2001).

31. Lehmann, M. F., Bernasconi, S. M., Barbieri, A. & McKenzie, J. A. Preservation of organic matter and alteration of its carbon and nitrogen isotope composition during simulated and in situ early sedimentary diagenesis. *Geochimica et Cosmochimica Acta* **66**, 3573–3584 (2002).
32. Stüeken, E. E. & Buick, R. Environmental control on microbial diversification and methane production in the Mesoarchean. *Precambrian Research* **304**, 64–72 (2018).
33. van Zuilen, M. A. *et al.* Graphite and carbonates in the 3.8 Ga old Isua Supracrustal Belt, southern West Greenland. *Precambrian Research* **126**, 331–348 (2003).
34. Johnson, C. M., Beard, B. L. & Roden, E. E. The Iron Isotope Fingerprints of Redox and Biogeochemical Cycling in Modern and Ancient Earth. *Annu. Rev. Earth Planet. Sci.* **36**, 457–493 (2008).
35. Heimann, A. *et al.* Fe, C, and O isotope compositions of banded iron formation carbonates demonstrate a major role for dissimilatory iron reduction in ~2.5Ga marine environments. *Earth and Planetary Science Letters* **294**, 8–18 (2010).
36. van Zuilen, M. A., Lepland, A. & Arrhenius, G. Reassessing the evidence for the earliest traces of life. *Nature* **418**, 627–630 (2002).
37. McCollom, T. M. Laboratory Simulations of Abiotic Hydrocarbon Formation in Earth's Deep Subsurface. *Reviews in Mineralogy and Geochemistry* **75**, 467–494 (2013).
38. Stüeken, E. E., Boocock, T., Szilas, K., Mikhail, S. & Gardiner, N. J. Reconstructing Nitrogen Sources to Earth's Earliest Biosphere at 3.7 Ga. *Frontiers in Earth Science* **9**, (2021).
39. Swanner, E. D., Webb, S. M. & Kappler, A. Fate of cobalt and nickel in mackinawite during diagenetic pyrite formation. *American Mineralogist* **104**, 917–928 (2019).
40. Craig, J. R. & Scott, S. D. Chapter 5. SULFIDE PHASE EQUILIBRIA. in *Sulfide Mineralogy* (ed. Ribbe, P. H.) 124–233 (De Gruyter, 1976). doi:10.1515/9781501508332-008.

41. Steadman, J. A. *et al.* Synsedimentary to Early Diagenetic Gold in Black Shale-Hosted Pyrite Nodules at the Golden Mile Deposit, Kalgoorlie, Western Australia. *Economic Geology* **110**, 1157–1191 (2015).

42. Qiu, W. J., Zhou, M. & Williams-Jones, A. E. Numerical Simulation of the Self-Organizational Origin of Concentrically Zoned Aggregates of Siderite and Pyrite in Sediment-Hosted Massive Sulfide Deposits. *JGR Solid Earth* **129**, e2023JB028101 (2024).

43. Bektursunova, R. & L'Heureux, I. A reaction-transport model of periodic precipitation of pyrite in anoxic marine sediments. *Chemical Geology* **287**, 158–170 (2011).

44. Farquhar, J., Bao, H. & Thiemens, M. Atmospheric Influence of Earth's Earliest Sulfur Cycle. *Science* **289**, 756–758 (2000).

45. Farquhar, J., Wu, N., Canfield, D. E. & Oduro, H. Connections between Sulfur Cycle Evolution, Sulfur Isotopes, Sediments, and Base Metal Sulfide Deposits. *Economic Geology* **105**, 509–533 (2010).

46. Ono, S. *et al.* New insights into Archean sulfur cycle from mass-independent sulfur isotope records from the Hamersley Basin, Australia. *Earth and Planetary Science Letters* **213**, 15–30 (2003).

47. Stetter, K. O. & Gaag, G. Reduction of molecular sulphur by methanogenic bacteria. *Nature* **305**, 309–311 (1983).

48. Surkov, A. V., Böttcher, M. E. & Kuever, J. Sulphur isotope fractionation during the reduction of elemental sulphur and thiosulphate by *Dethiosulfovibrio* spp. *Isotopes in Environmental and Health Studies* **48**, 65–75 (2012).

49. Canfield, D. E. & Raiswell, R. The evolution of the sulfur cycle. *American Journal of Science* **299**, 697–723 (1999).

50. Galić, A. *et al.* Pyrite in a sulfate-poor Paleoarchean basin was derived predominantly from elemental sulfur: Evidence from 3.2 Ga sediments in the Barberton Greenstone Belt, Kaapvaal Craton. *Chemical Geology* **449**, 135–146 (2017).
51. Johnston, D. T. Multiple sulfur isotope fractionations in biological systems: A case study with sulfate reducers and sulfur disproportionators. *American Journal of Science* **305**, 645–660 (2005).
52. Frei, R. & Polat, A. Source heterogeneity for the major components of ~3.7 Ga Banded Iron Formations (Isua Greenstone Belt, Western Greenland): Tracing the nature of interacting water masses in BIF formation. *Earth and Planetary Science Letters* **253**, 266–281 (2007).
53. Papineau, D. & Mojzsis, S. J. Mass-independent fractionation of sulfur isotopes in sulfides from the pre-3770 Ma Isua Supracrustal Belt, West Greenland. *Geobiology* **4**, 227–238 (2006).
54. Whitehouse, M. J. Multiple Sulfur Isotope Determination by SIMS: Evaluation of Reference Sulfides for Δ33S with Observations and a Case Study on the Determination of Δ36S. *Geostandards and Geoanalytical Research* **37**, 19–33 (2013).
55. Macdonald, J. E. *et al.* Evaluating the multiple sulfur isotope signature of Eoarchean rocks from the Isua Supracrustal Belt (Southwest-Greenland) by MC-ICP-MS: Volcanic nutrient sources for early life. *Geobiology* **22**, e12595 (2024).
56. Shen, Y., Farquhar, J., Masterson, A., Kaufman, A. J. & Buick, R. Evaluating the role of microbial sulfate reduction in the early Archean using quadruple isotope systematics. *Earth and Planetary Science Letters* **279**, 383–391 (2009).
57. Roerdink, D. L., Mason, P. R. D., Farquhar, J. & Reimer, T. Multiple sulfur isotopes in Paleoarchean barites identify an important role for microbial sulfate reduction in the early marine environment. *Earth and Planetary Science Letters* **331–332**, 177–186 (2012).

58. Roerdink, D. L., Mason, P. R. D., Whitehouse, M. J. & Brouwer, F. M. Reworking of atmospheric sulfur in a Paleoarchean hydrothermal system at Londozi, Barberton Greenstone Belt, Swaziland. *Precambrian Research* **280**, 195–204 (2016).

59. Farquhar, J. *et al.* Pathways for Neoarchean pyrite formation constrained by mass-independent sulfur isotopes. *Proc. Natl. Acad. Sci. U.S.A.* **110**, 17638–17643 (2013).

60. Williford, K. H., Van Kranendonk, M. J., Ushikubo, T., Kozdon, R. & Valley, J. W. Constraining atmospheric oxygen and seawater sulfate concentrations during Paleoproterozoic glaciation: In situ sulfur three-isotope microanalysis of pyrite from the Turee Creek Group, Western Australia. *Geochimica et Cosmochimica Acta* **75**, 5686–5705 (2011).

61. Mojzsis, S. J., Coath, C. D., Greenwood, J. P., McKeegan, K. D. & Harrison, T. M. Mass-independent isotope effects in Archean (2.5 to 3.8 Ga) sedimentary sulfides determined by ion microprobe analysis. *Geochimica et Cosmochimica Acta* **67**, 1635–1658 (2003).

62. Bullock, E. S., McKeegan, K. D., Gounelle, M., Grady, M. M. & Russell, S. S. Sulfur isotopic composition of Fe-Ni sulfide grains in CI and CM carbonaceous chondrites. *Meteorit & Planetary Scien* **45**, 885–898 (2010).

63. Ding, T. *et al.* Calibrated sulfur isotope abundance ratios of three IAEA sulfur isotope reference materials and V-CDT with a reassessment of the atomic weight of sulfur. *Geochimica et Cosmochimica Acta* **65**, 2433–2437 (2001).

Figure 1. Carbon isotopic variations, total organic carbon concentrations and iron concentrations. Errors are smaller than the symbol size. Pelagic samples are characterized by fine layering, whereas turbiditic samples are characterized by unstructured or graded layers, generally thicker than 1 cm. a) Carbon isotopic variation and TOC. Samples with high TOC generally have heavier $\delta^{13}C$. $\delta^{13}C$ lower than −30‰ are only observed in low TOC samples. b) Carbon isotopic variation and Fe/TOC. $\delta^{13}C$ shows a negative trend with Fe/TOC, suggesting that the amount of light carbon remaining in the samples was controlled by the availability of Fe^{3+} for respiration during

seafloor diagenesis. Some samples with moderate or low Fe/TOC and light $\delta^{13}C$ suggest that additional oxidants were available for respiration, such as S^0 or SO_4^{2-}.

Figure 2. Optical micrographs of polished thin sections.
Images are from the following depths in the rock core: 11.84m (a), 26.63m (b), 34.96m (c), 37.07m (d) and 32.48m (e). a) Layers consisting of graphite (Gr) and muscovite (Ms) divided by layers of quartz (Qtz). Thicker layers in the middle contain pyrrhotite (Po; opaque) and calcite (Cal; outlined in blue). b) Reflected light image of layers with variable chlorite (Chl) and quartz (Qtz) content (boundaries shown by orange stippled lines) separated by biotite (Bt) rich layer with a thinner layer consisting of clinozoisite (Czo) grains. Clinozoisite likely formed under metamorphic conditions, along a bed containing Fe^{3+}-bearing minerals. c) Pyrrhotite (Po) grains in the upper half (opaque) along quartz (Qtz) rich bed, between graphite (Gr) bearing layers with muscovite (Ms), chlorite (Chl) and quartz. High quartz concentration may indicate a period of slow detrital deposition, allowing the accumulation of chert and sulfurous phases. d) A thin bed of pyrrhotite (Po; opaque) extending along the boundary between layers slightly variable proportions of quartz (Qtz), chlorite (Chl), biotite (Bt), albite (Ab) and graphite (Gr). e) Reflected light image of a large amalgamation of pyrrhotite (Po) and pyrite (Py; middle) situated between quartz-rich layers. Concentrically layered pyrite nodules may represent pre-metamorphic textures formed where H_2S and Fe^{2+} bearing fluids meet (see main text for implications).

Figure 3. Schematic illustration of processes taking place above and below the ISB seafloor.
Organic detritus is deposited within sedimentary layers and degrades through organic or inorganic processes into organic acids and methane (C_{org} and CH_4). Microbes respire these compounds anaerobically using Fe^{3+}, sulfate, or possibly elemental sulfur as oxidants, while elemental sulfur may also have undergone microbial disproportionation ($S + 4H_2O \rightarrow SO_4^{2-} + 3H_2S + 2H^+$). Resultant H_2S and Fe^{2+} react to form iron sulfides. Fe^{2+} may have been supplied both by microbial Fe reduction within the sediments and from seawater. If H_2S is in excess it may migrate and form iron sulfides upon contact with Fe^{2+} from seawater, as suggested by sulfide petrography (see main text). Respiration also generates HCO_3^-, which combines with porewater Ca^{2+}, or other metals, to precipitate carbonate. Fe^{3+} is derived from photoferrotrophy in the water column, while elemental sulfur and sulfate are thought to originate from photochemical disproportionation of atmospheric SO_2 under anoxic conditions.

Figure 4. Sulfur isotopic compositions of sulfide minerals plotted as $\delta^{34}S$ versus $\Delta^{33}S$.
Errors represent 1σ. All sulfide phases (pyrrhotite, pyrite, pentlandite, chalcopyrite) within individual sections covering (0.5cm to 4cm), have $\Delta^{33}S$ within error of each other, consistent with metamorphic phases inheriting local $\Delta^{33}S$ values. Concentrically zoned pyrite generally displays wider ranges in $\delta^{34}S$ and reach more negative values (see Fig. S2; Supplementary data 2;), consistent with these grains having experienced less isotopic equilibration under metamorphic conditions. The variation may be caused by mineral formation or fractionation during reduction of sulfur phases to sulfide. Isotopic data representing the most positive[54] and most negative $\Delta^{33}S$[55] may be representative of mixing endmembers that explain the range of data measured. The Archean Reference Array, represented by the bold black line, is discussed in the main text.

Editorial summary:
Organic debris from organisms living in the ocean water column was used as substrate for microbes carrying out anaerobic respiration within the oldest known detrital sediments on Earth, according to isotopic and petrological analysis.

Peer review information:

Communications Earth and Environment thanks Takeshi Kakegawa and the other, anonymous, reviewer(s) for their contribution to the peer review of this work. Primary Handling Editor: Alireza Bahadori. A peer review file is available.

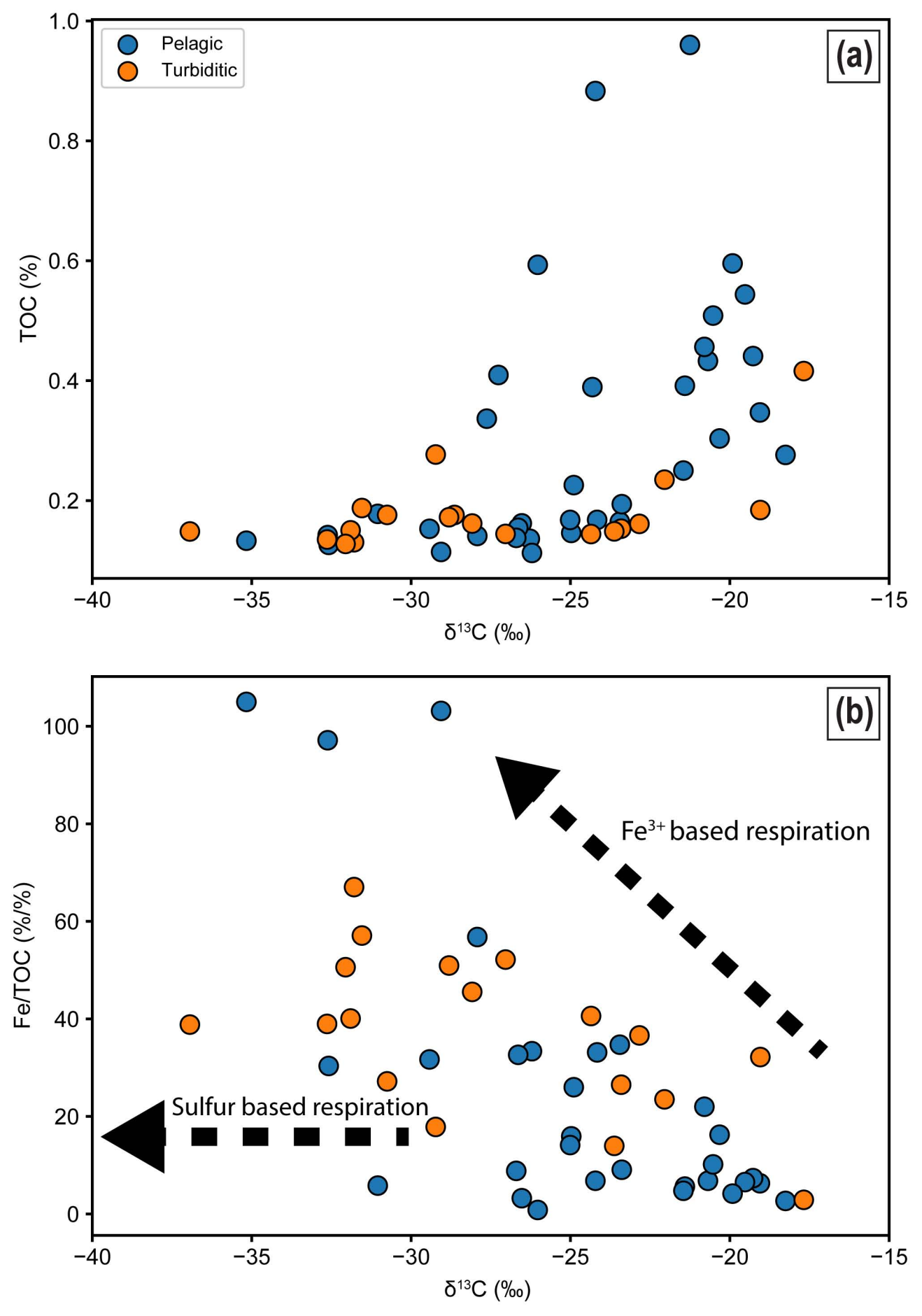
(a)
Pelagic
Turbiditic
TOC (%)
1.0
0.8
0.6
0.4
0.2
−40
−35
−30
−25
−20
−15
δ13C (‰)
(b)
Fe3+ based respiration
Sulfur based respiration
Fe/TOC (%/%)
100
80
60
40
20
0
−40
−35
−30
−25
−20
−15
δ13C (‰)

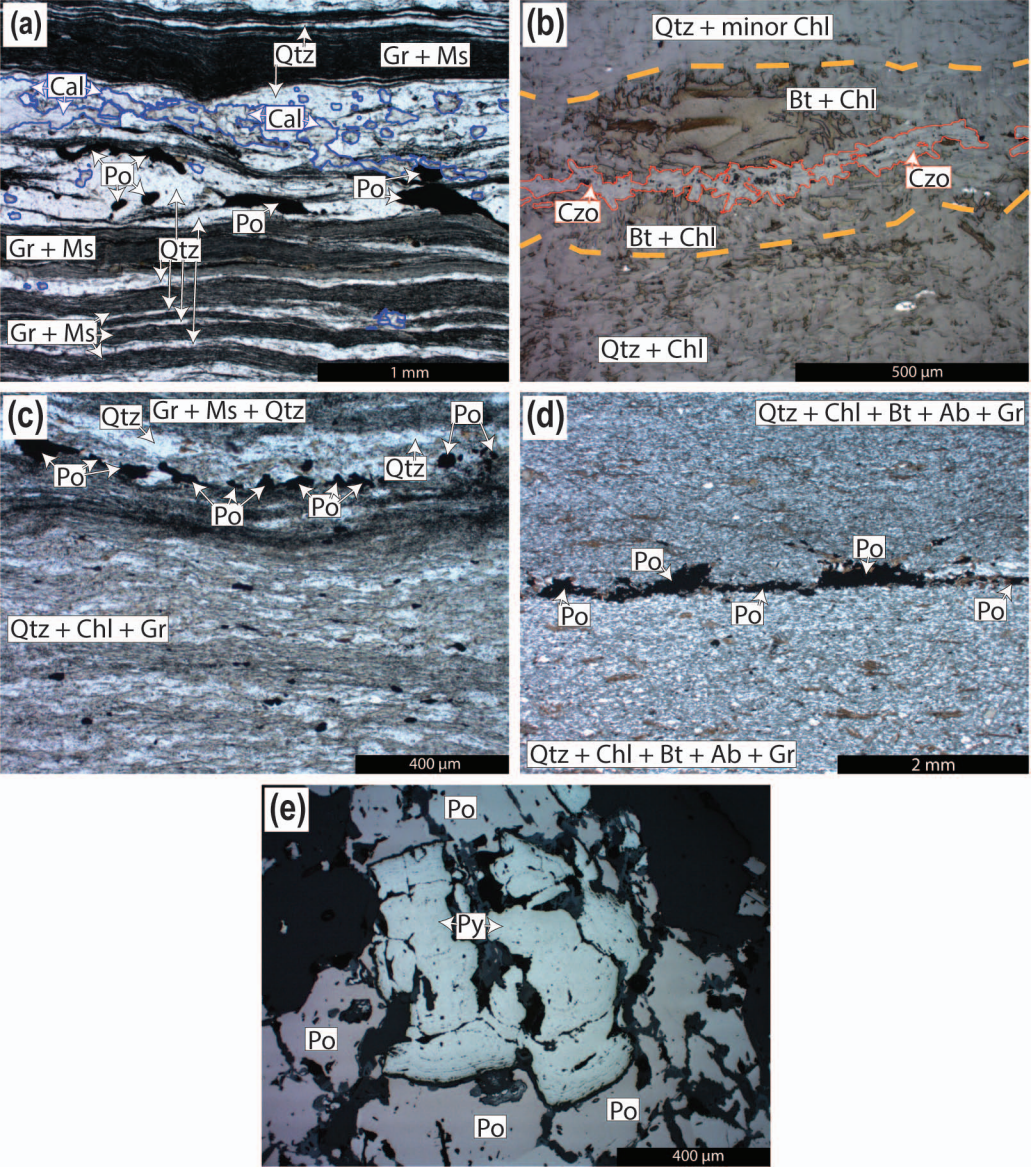
(a)
Qtz
Gr + Ms
Cal
Cal
Po
Po
Po
Gr + Ms
Qtz
Gr + Ms
1 mm
(b)
Qtz + minor Chl
Bt + Chl
Czo
Czo
Bt + Chl
Qtz + Chl
500 µm
(c)
Qtz
Gr + Ms + Qtz
Po
Po
Qtz
Po
Po
Qtz + Chl + Gr
400 µm
(d)
Qtz + Chl + Bt + Ab + Gr
Po
Po
Po
Po
Po
Qtz + Chl + Bt + Ab + Gr
2 mm
(e)
Po
Py
Po
Po
Po
400 µm

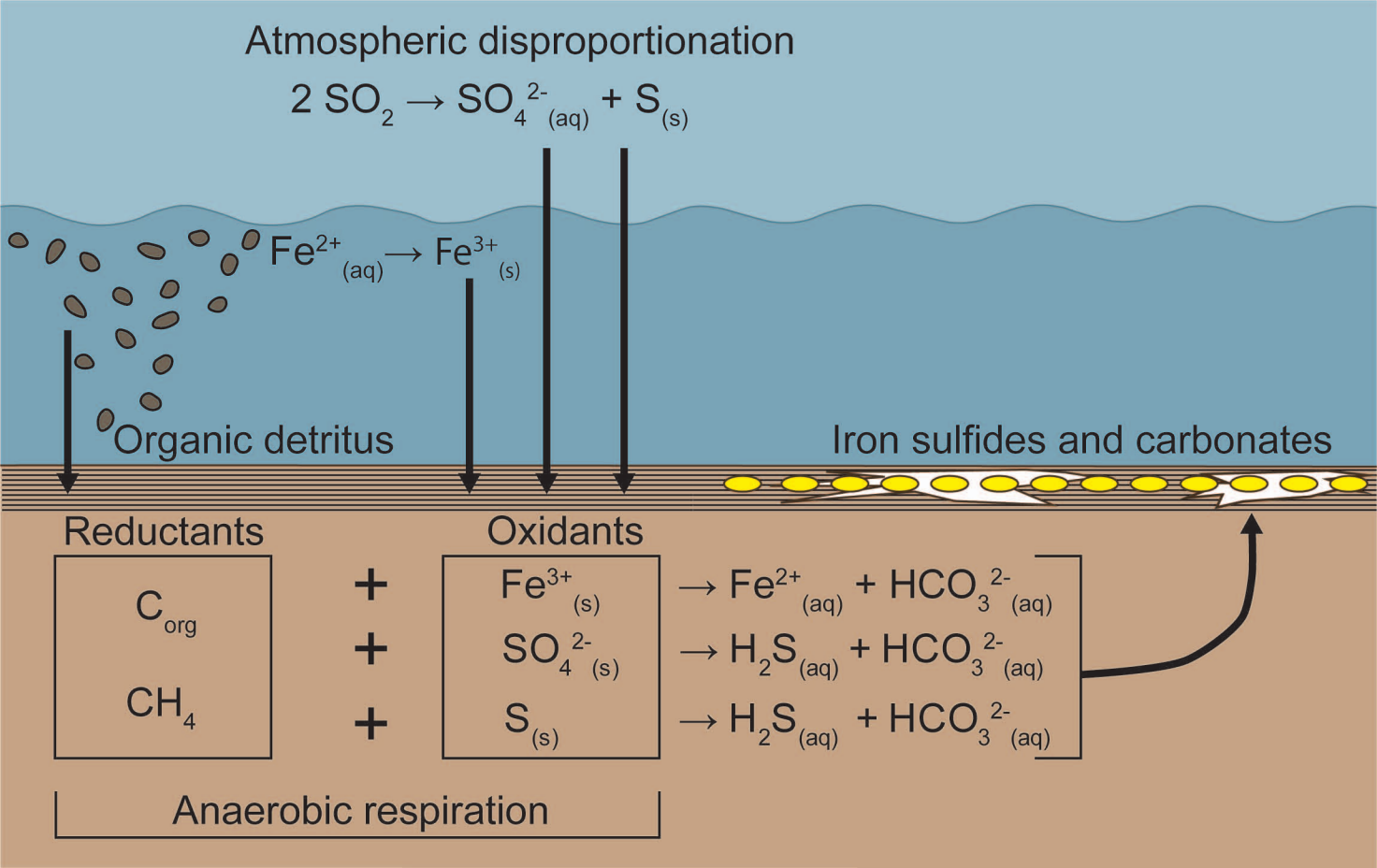
Atmospheric disproportionation
2 SO2 → SO4 2- (aq) + S (s)
Fe2+ (aq) → Fe3+ (s)
Organic detritus
Iron sulfides and carbonates
Reductants
Oxidants
Corg
CH4
+
+
+
Fe3+ (s) → Fe2+ (aq) + HCO3 2- (aq)
SO4 2- (s) → H2S (aq) + HCO3 2- (aq)
S (s) → H2S (aq) + HCO3 2- (aq)
Anaerobic respiration

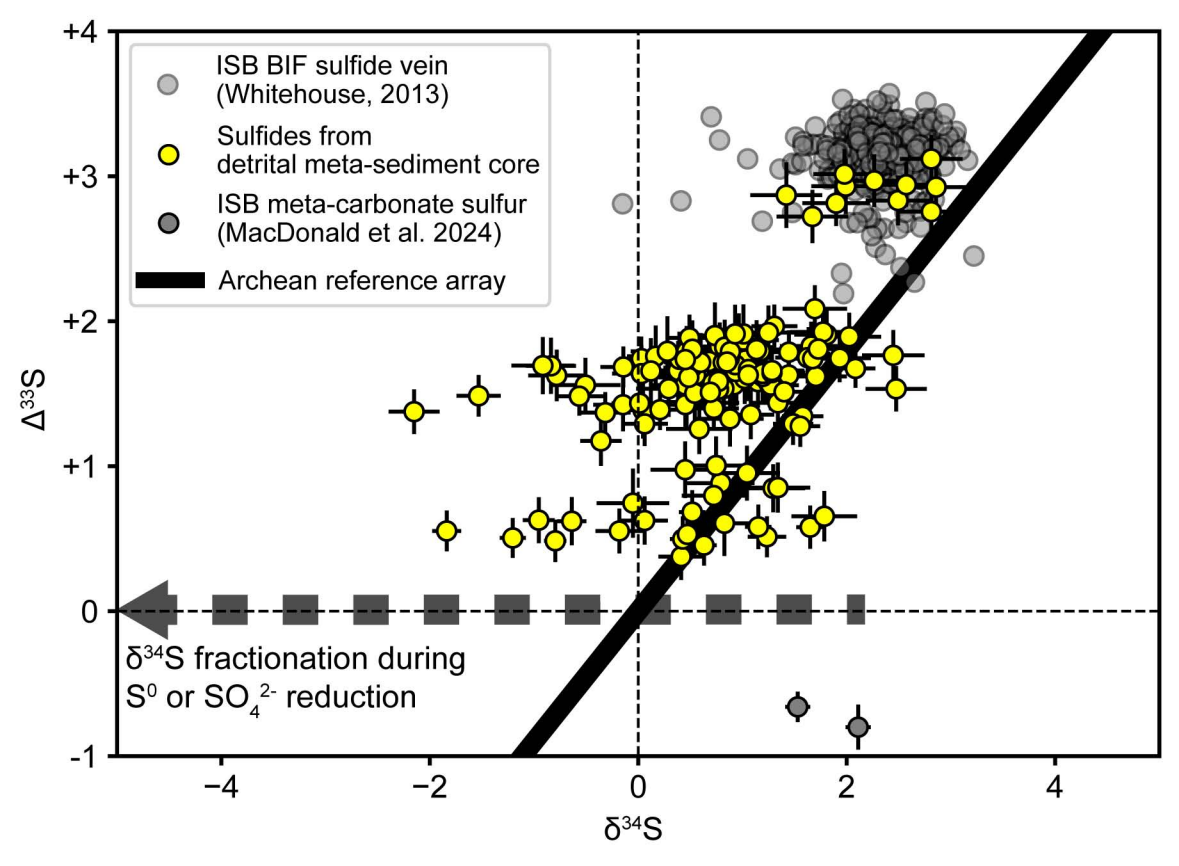
ISB BIF sulfide vein
(Whitehouse, 2013)
Sulfides from
detrital meta-sediment core
ISB meta-carbonate sulfur
(MacDonald et al. 2024)
Archean reference array
δ34S fractionation during
S0 or SO4 2- reduction
Δ33S
δ34S
+4
+3
+2
+1
0
-1
−4
−2
0
2
4